Mon. Not. R. Astron. Soc. **262**, 93–108 (1993)

Discovery of an EUV-bright polar in the period gap from the *ROSAT* Wide Field Camera sky survey

D. A. H. Buckley,[1] D. O'Donoghue,[2] B. J. M. Hassall,[3] B. J. Kellett,[4] K. O. Mason,[5] K. Sekiguchi,[1] M. G. Watson,[6] P. J. Wheatley[6] and A. Chen[2]

[1] *South African Astronomical Observatory, PO Box 9, Observatory 7935, South Africa*
[2] *Astronomy Department, University of Cape Town, Rondebosch 7700, South Africa*
[3] *Royal Greenwich Observatory, Madingley Road, Cambridge CB3 0EZ*
[4] *Astrophysics Division, Rutherford Appleton Laboratory, Chilton, Didcot, Oxon. OX11 0QX*
[5] *Mullard Space Science Laboratory, University College London, Holmbury St Mary, Dorking, Surrey RH5 6NT*
[6] *X-ray Astronomy Group, Department of Physics and Astronomy, University of Leicester, Leicester LE1 7RH*

Accepted 1992 October 20. Received 1992 October 13; in original form 1992 August 24

ABSTRACT

We report the discovery of a new polar found during the all-sky survey of extreme-UV sources conducted by the UK Wide Field Camera on board *ROSAT*. The $V \sim 16$ object is the brightest EUV polar observed by this instrument during the survey. These and subsequent optical observations show that the orbital period of the system is 2.33 h, placing it well inside the cataclysmic variable 'period gap'. Results from preliminary optical photometry, spectroscopy and polarimetry are presented, and compared to other known polars. The *ROSAT* results indicate that the system exhibits a soft X-ray excess, by at least a factor of ~ 2 over the hard bremsstrahlung component. We discuss the likely evolutionary status of this 'period gap' polar, and conclude that it was probably born in the gap, rather than evolving through it from a longer period. Finally, we discuss the probable accretion geometry of the system.

Key words: accretion, accretion discs – surveys – stars: individual: RE 1938 – 461 – stars: magnetic fields – novae, cataclysmic variables – X-rays: stars.

1 INTRODUCTION

Polars, or AM Herculis binaries, are a class of magnetic cataclysmic variables (CVs) containing synchronously, or almost synchronously, rotating and strongly magnetic ($B \sim 10$–60 MG) accreting white dwarfs (see reviews, e.g. Lamb & Melia 1988; Wickramasinghe 1988; Schmidt 1988; Beuermann 1988; Cropper 1990). The magnetospheric radius (or Alfvén radius) of the white dwarf is large enough at least to prevent accretion disc formation, and for the magnetic field to influence the accretion at a distance from the white dwarf of order the binary separation. The gas lost from the secondary star through the inner Lagrangian point (L1) is eventually channelled on to confined regions of the white dwarf's surface, at the footprints of the field lines near one or both of the magnetic poles. The fast quasi-radial inflow results in an accretion 'column' of ionized gas, which produces a strong shock just above the surface, and subsequently cools predominantly by thermal bremsstrahlung emission of hard X-rays ($kT > 10$ keV). A substantial fraction of this hard X-ray flux is absorbed, thermalized, and re-radiated from a region of the white dwarf's surface directly under, or close to, the accretion column. Mechanical heating by accreting matter that penetrates the photosphere directly may also be important. This re-radiated energy is characterized as a blackbody emitting principally in the soft X-ray/EUV part of the spectrum, and may constitute the dominant fraction of the polar's luminosity. Electrons in or near the accretion column spiral around the magnetic field lines, emitting beamed cyclotron radiation which is strongly polarized. The characteristic field strength of ~ 10–60 MG results in this cyclotron component being emitted in the optical to infrared region.

The first all-sky survey at EUV wavelengths (0.01–0.2 keV) was carried out using the UK Wide Field Camera (WFC; Wells et al. 1990) on board *ROSAT*, from 1990 July, and was 98 per cent completed by 1991 February. Because the bulk of the accretion luminosity of polars is released in the soft X-ray/EUV region, it was predicted that a large number (50–100) of new polars would be identified (e.g.

King, Hameury & Lasota 1990; Hameury, King & Lasota 1990) from the EUV survey. To date, six new discoveries have added to the 17 polars already known. In this paper we report the discovery of the brightest of *all* the polars in the EUV, RE 1938−461. Furthermore, from the EUV and optical light curves, and the radial velocity variations, we have determined its orbital period to be 2.33 h, placing it well within the CV 'period gap' where there is a dearth of CVs, i.e. four confirmed systems well inside the gap (V Per, V795 Her, 1H 0709−360 and TU Men).

2 OPTICAL IDENTIFICATION

We are involved in a systematic programme to identify the optical counterparts of all the *ROSAT* EUV sources observed during the WFC survey (Mason et al. 1991). A catalogue of the 384 brightest sources detected during the survey, including many identifications, will appear shortly (Pounds et al. 1993). The identification procedure first consists of producing finding charts from COSMOS scans of UK Schmidt survey plates (at southern declinations), sometimes in two filters, which include stars to a limiting magnitude of ~24. Then all candidate stars within a WFC source error circle are observed spectroscopically until a likely identification is made.

A star with a COSMOS J-magnitude (blue) of ~14.4 was found within the 41 arcsec (90 per cent confidence) radius error circle of the source RE 1938−461 (Fig. 1). It was observed on 1991 July 9 at the South African Astronomical Observatory (SAAO) using the 1.9-m telescope, equipped with the ITS spectrograph and the two-channel photon-counting Reticon detector (RPCS). A low-resolution spectrum ($\Delta\lambda \sim 6$ Å) covering $\lambda\lambda$3500–7000 Å was obtained, which is shown in Fig. 2. Intense emission lines of the Balmer series, He II λ4686 Å, and strong H I lines ($\lambda\lambda$4027, 4388, 4471, 4713, 4922, 5015, 5411, 5876, 6678) are seen superimposed on a blue continuum which has a large Balmer jump in emission. The spectrum is typical of a cataclysmic variable, while the line intensities, and specifically both the strength of He II λ4686 Å and the Balmer jump, indicate a *magnetic* CV classification. Also of note is the O III λ3444-Å Bowen fluorescence line, a common feature in polar spectra. In Table 1 we list the emission-line parameters determined from Gaussian fits to the line profiles. Internal errors are typically ±10 per cent, while fluxes are probably accurate to better than 20 per cent.

3 OPTICAL OBSERVATIONS

Immediately following its optical identification, RE 1938−461 was the subject of an intense follow-up programme of optical observations at the SAAO, including high-

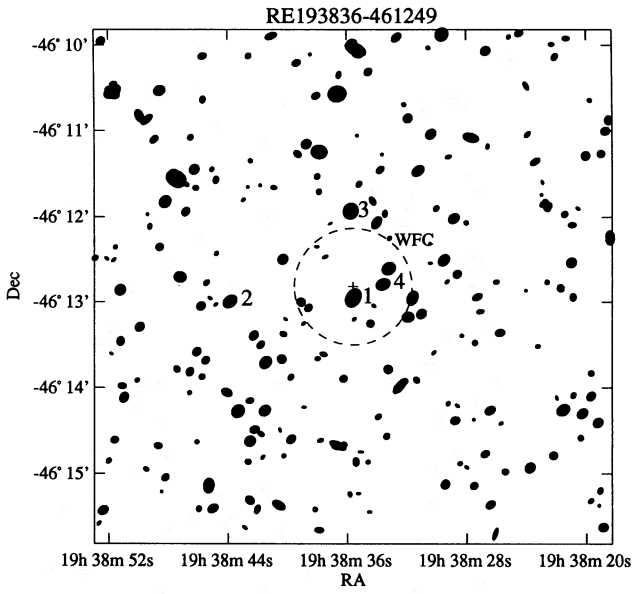

Figure 1. Finding chart (~6×6 arcmin^2) for RE 1938−461 produced from COSMOS scans of UKSTU plates. The dashed circle is the 90 per cent confidence position of the WFC source, and the optical counterpart is labelled 1, while the three CCD frame standards are labelled 2–4. The COSMOS position of the polar (star #1) is RA=19^{h}38^{m}35^s.6, Dec.=−46°12′57″.2 (Equinox 2000), and the uncertainties are likely to be ~0.6 arcsec.

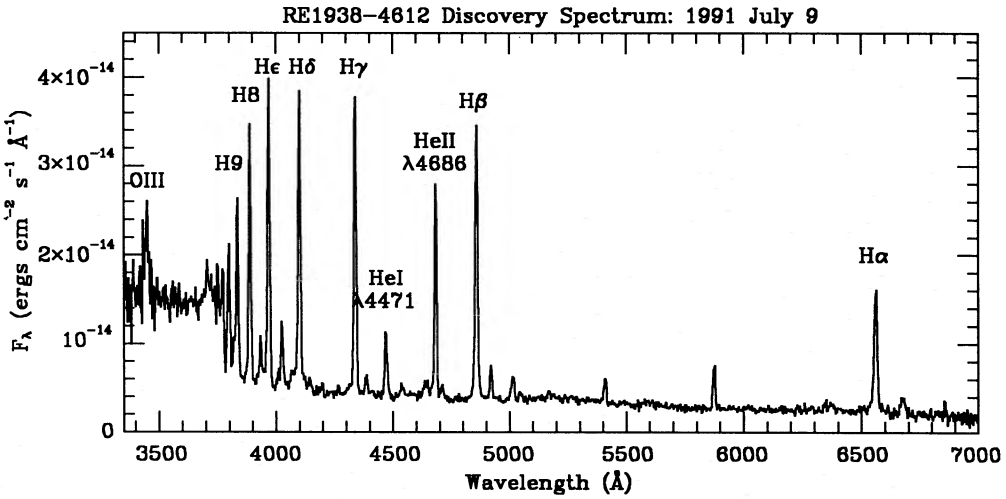

Figure 2. Discovery spectrum ($\Delta\lambda \sim 6$ Å) of RE 1938−461, obtained on 1991 July 9 with the RPCS and Unit spectrograph on the SAAO 1.9-m telescope.

Table 1. RE 1938 − 461 emission-line parameters.

Line	Peak Intensity (ergs cm^{-2} s^{-1}Å^{-1})	Flux (ergs cm^{-2} s^{-1})	FWHM (Å)	E.W. (Å)
H10	1.42 ± 0.13 × 10^{-14}	2.14 × 10^{-13}	11.3 ± 0.8	30.6
H9	1.85 ± 0.09 × 10^{-14}	2.73 × 10^{-13}	11.1 ± 0.4	41.5
H8	2.75 ± 0.20 × 10^{-14}	3.85 × 10^{-13}	10.4 ± 0.5	64.5
CaII	4.41 ± 0.20 × 10^{-15}	4.89 × 10^{-14}	8.5 ± 0.4	7.7
Hε/CaII	3.35 ± 0.01 × 10^{-14}	5.20 × 10^{-13}	11.2 ± 0.1	4.6
HeIλ4027	7.00 ± 0.07 × 10^{-15}	8.87 × 10^{-14}	9.6 ± 0.1	15.9
Hδ	3.16 ± 0.22 × 10^{-14}	4.95 × 10^{-13}	11.6 ± 0.5	82.8
Hγ	3.22 ± 0.21 × 10^{-14}	4.81 × 10^{-13}	11.3 ± 0.4	101.9
HeIλ4387	2.05 ± 0.25 × 10^{-15}	3.35 × 10^{-14}	12.1 ± 1.6	47.6
HeIλ4471	7.11 ± 0.02 × 10^{-15}	1.16 × 10^{-13}	12.1 ± 0.1	28.3
HeIIλ4686	2.34 ± 0.17 × 10^{-14}	3.16 × 10^{-13}	10.2 ± 0.4	69.1
Hβ	2.75 ± 0.18 × 10^{-14}	4.68 × 10^{-13}	13.0 ± 0.5	121.6
HeIλ4922	3.62 ± 0.04 × 10^{-15}	4.73 × 10^{-14}	9.8 ± 0.1	12.1
HeIλ5015	2.83 ± 0.09 × 10^{-15}	5.54 × 10^{-14}	14.7 ± 0.6	15.6
HeIIλ5411	2.88 ± 0.41 × 10^{-15}	4.46 × 10^{-14}	11.6 ± 1.7	13.2
HeIλ5876	4.99 ± 0.04 × 10^{-15}	8.40 × 10^{-14}	12.6 ± 0.1	32.0
Hα	1.29 ± 0.08 × 10^{-14}	2.74 × 10^{-13}	15.8 ± 0.6	109.5
HeIλ6678	1.88 ± 0.18 × 10^{-15}	6.11 × 10^{-14}	23.9 ± 3.9	30.6

speed photometry, CCD photometry, time-resolved spectroscopy, and polarimetry. A complete log of the observations is given in Table 2.

3.1 High-speed photometry

Continuous white-light photometry of RE 1938 − 461 was undertaken on 1991 August 8, 9 and 11 using the University of Cape Town photometer (UCTP) on the SAAO 0.75-m telescope and the St Andrews Photometer (StAP) on the 1.0-m telescope. Blue sensitive photomultipliers were used (S11 photocathodes): an EMI 6256 on the StAP and an Amperex 56DVP on the UCTP. For blue objects like CVs, such white-light photometry is approximately equivalent to *B*-band observations. The integration time was 10 s, and the sky was monitored regularly (every 15–20 min). The data were reduced by fitting a spline to the sky values, which was then subtracted from the star values, followed by atmospheric extinction correction using a mean extinction coefficient. Light curves for the three nights are shown in Fig. 3, together with the two nights' high-speed photometry extracted from the polarimetry observations (Section 3.4). The data displayed in Fig. 3 have been binned to a time resolution of 30 s and normalized, by first subtracting and then dividing by the mean nightly count rate. The fit will be discussed in Section 6.

3.2 Spectroscopy

Spectroscopy of RE 1938 − 461, using the 1.9-m telescope with the same instrumentation previously described, was undertaken on 1991 August 9 and 10, and September 5. The August observations employed an 830 line mm^{-1} grating blazed at ~3900 Å in order II, which gave a resolution of ~1.2 Å and a wavelength coverage from ~4300 to 4800 Å. For the September observations, a 1200 line mm^{-1} grating with ~2-Å resolution was used, with an effective blaze at ~4600 Å, and covering ~4000 to 5000 Å. For all of these observations, the RPCS was run in a semi-continuous mode, with 300-s star exposures. Regular (i.e. every 1000–2000 s) calibration arc exposures of 100 s were obtained during the observing runs. All of the data were reduced in a similar manner: first they were flat-field corrected, and then wavelength-calibrated using polynomial fits to the arc spectra. Finally, the sky spectrum was subtracted from the object spectrum.

3.3 CCD photometry

Further photometry of RE 1938 − 461, using the UCL CCD camera on the SAAO 1.0-m telescope, was undertaken on 1991 August 29. For these observations, *B*, R_c and I_c frames were taken in a semi-continuous manner, from ~23:42 to 02:50 UT. *B*-band exposures of 100 s were followed by 25-s *R* exposures, and then five consecutive 50-s *I* exposures. This cycle was then repeated for the duration of the run. The aim of these initial CCD observations was to investigate if the longer wavelength (*R*, *I*) light curves were substantially different from the *B*-band, and previously obtained 'blue' high-speed photometry, light curves. Such differences may indicate the presence of secondary emission regions, as in the purported polar Grus V1 (Tuohy et al. 1988).

Table 2. Log of the optical observations.

Run	Date (1991)	HJD range (+2440000)	Duration (hours)	Filter	Int.Time (sec)
High-Speed Photometry:					
S5372	Aug 8/9	8477.3922 - .5589	4.00	white	10
S5361	Aug 9/10	8478.2496 - .5459	7.11	white	10
S5380	Aug 11/12	8480.2317 - .4882	6.15	white	10
Polarimetry/Photometry					
P8500	Aug 31/1	8500.3027 - .5679	6.37	white	10/120
P8501	Sep 1/2	8501.3002 - .5440	5.85	white	10/120
P8502	Sep 2/3	8502.2787 - .5557	6.65	white	10/120
CCD Photometry					
DB01	Aug 29/30	8498.4922 - .5858	2.25	B	100
		8498.5039 - .6027	2.37	R	25
		8498.5046 - .6057	2.43	I	50
KOM01	Oct 1/2	8531.2872 - .4473	3.84	V	120
KOM02	Oct 4/5	8534.2347 - .3807	3.50	V	90/120
KOM03	Oct 5/6	8535.2651 - .4473	4.37	V	120
Time Resolved Spectroscopy					
R8478	Aug 9/10	8478.4570 - .5908	3.37	-	300
R8480	Aug 11/12	8480.4766 - .5928	2.79	-	300
R8504	Sep 5/6	8505.4355 - .5566	2.91	-	300

All of the 108 CCD frames obtained were reduced in an identical manner with initial flat-fielding, bias removal, and correction for pre-flashing. The frames were then processed using the DoPHOT reduction package (Mateo & Schechter 1989), where both fit and aperture magnitudes were determined. Three stars on the frames were used to define a canonical frame standard, which was then used to derive B, R_c and I_c magnitudes of all stars, relative to this canonical standard. These comparison stars are indicated on the finding chart (Fig. 1) and are labelled # 2, # 3 and # 4. Their magnitudes were derived after zero-point corrections using observations of E-region standards (Menzies et al. 1989) at the end of the night, and are listed in Table 3. We show the light curves for RE 1938−461 in Fig. 4, and include for comparison the I-band light curves for the three comparisons, whose mean defined the canonical frame standard. We note that the rms scatter of these comparison differential light curves is <0.01 mag. Notwithstanding the poorer temporal resolution of the B light curve, we can say that, in comparison, the longer wavelength (R, I) light curves look morphologically no different.

Further CCD photometry, in the V band, was undertaken using the same instrumentation on 1991 October 1, 4 and 5. The frames were cleaned in the manner described above, and were then reduced by fitting one-dimensional Gaussians in the y-direction to star images compressed in the x-direction, superimposed on a flat local background. The frames were calibrated using comparison star # 3 as a local frame standard, which was in fact one of the three stars used to define the canonical comparison in the August 29 observation. The V magnitude derived for this star is 15.13, with a probable external error of ~ 0.1. In Fig. 5 we present three V light curves for RE 1938−461.

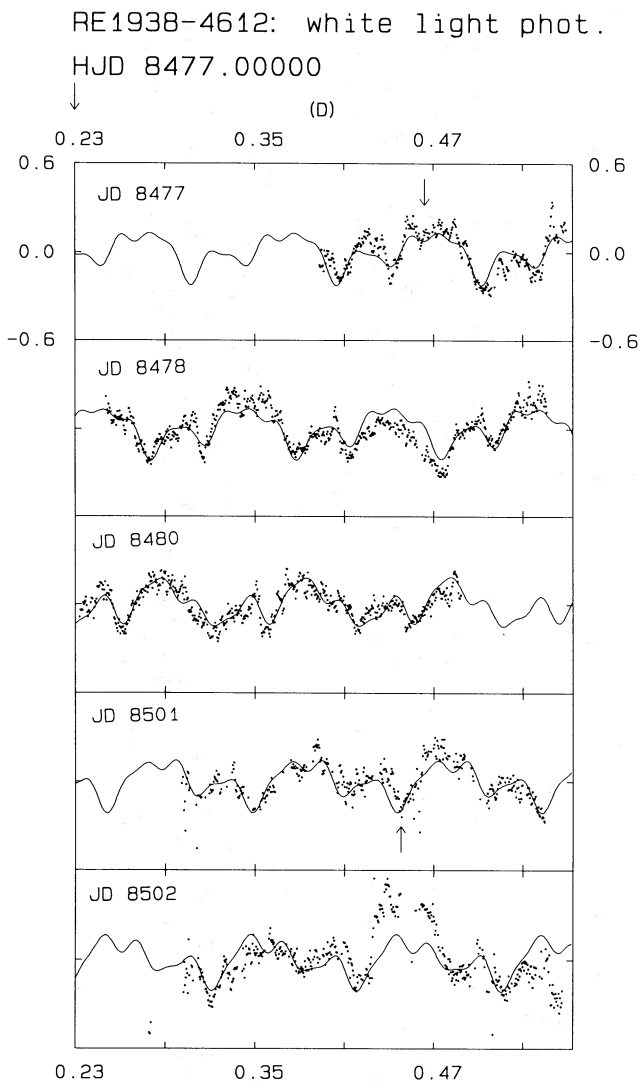

Figure 3. White-light photometry of RE 1938−461 obtained on 1991 August 8, 9, 11, September 1 and 2 with the SAAO 0.75-m and 1.0-m telescopes (see log in Table 2). The abscissa is in fractional Julian days, and the integer part is at the top left of each panel. The ordinate is the intensity after subtraction and division by the nightly mean and therefore the range is ±60 per cent of the mean intensity. The data have been binned to a resolution of 30 s, and the last two light curves (September) were extracted from the polarimetry observations. A non-linear least-squares fit of three sinusoids is also shown, with the dominant frequency at 0.119 025 mHz, and two other frequencies close to the harmonics (see text and Table 5). The time of maximum light used in the ephemeris is indicated by an arrow in the top panel, while the time of primary minimum used to bin the data (Fig. 14) is shown by the arrow in the panel for JD 8501.

Table 3. Magnitudes of comparison stars.

Star	B	σ_B	R	σ_R	I	σ_I
Comp #2	16.364	0.015	14.932	0.013	14.470	0.025
Comp #3	15.642	0.014	14.770	0.017	14.480	0.008
Comp #4	16.424	0.024	15.478	0.011	14.145	0.022

3.4 Polarimetry

RE 1938−461 was observed on 1991 August 31, September 1 and 2, using the UCT Polarimeter on the SAAO 1.0-m telescope. The Polarimeter employs both 1/4- and 1/2-waveplate superachromat retarders, in conjunction with a Glan–Thomson analyser, and is fully described by Cropper (1985). White light observations were made using a cooled, red-sensitive ($\lambda\lambda$3000–11 000 Å) GaAs photomultiplier (RCA 31035A). The data acquisition program was run in a manner which allowed consecutive 10-s integrations for the intensity measurements, while the resolution for the polarization measurements was ~120 s. Whereas the first night's data were obtained in conditions of poor seeing, and with occasional cirrus clouds, and consequently unphotometric, the subsequent two nights were of photometric quality.

Polarization results for each night show typical variations of between 2 and 10 per cent for linear, and 1 and 6 per cent for circular, with a scatter of $< \sim 1$ per cent. Distinct variations in both linear and circular polarization are observed, which, for the latter at least, are shown to occur at the orbital period (Section 8). The detection of variable circular polarization establishes beyond doubt that RE 1938−461 is indeed an AM Her-type CV (a polar). We will postpone a discussion of the polarization variations until later, and for now we just present the white light photometry, of which the light curves for the two photometric nights are included in Fig. 3. The mean V magnitude during the two photometric nights was ~15.6, similar to the CCD results.

4 *ROSAT* WFC OBSERVATIONS

RE 1938−461 was observed by the *ROSAT* WFC for 7.1 days during the all-sky survey, between 1990 September 26 and October 3. The survey coverage provides brief 'snapshot' measurements every 96 min each time the WFC field of view scans across the source, with integrations for each snapshot ranging from ~10 to 78 s. Survey observations were made with the two WFC survey filters, S1a (90–210 eV) and S2a (61–111 eV), alternating at 1-d intervals, yielding cumulative integration times of 1166 s in the S1 filter, and 870 s in the S2 filter.

RE 1938−461 is one of the brightest new sources discovered in the *ROSAT* all-sky survey, bright enough for it to be easily detectable on many of the individual survey scans. The survey light curve for RE 1938−461 is shown in Fig. 6. In order to construct this light curve, source counts were accumulated in a detection cell with a radius optimized to give the best signal-to-noise ratio. A radius of 6 arcmin was used for the S1a filter and 4.7 arcmin for the S2a filter. The background light curve was determined using the average of two background regions, each the same size as the detection cell, and displaced either side of the source along the survey scan path. This approach has the advantage of ensuring that the background light curve is measured with the same region of the detector as the detection cell. Extensive tests have demonstrated that this technique provides the most reliable estimate for the WFC background in the survey. The light curve shown in Fig. 6 has been background-subtracted (using the background light curve renormalized to the area of the source detection cell), and has also been corrected for the varying exposure time,

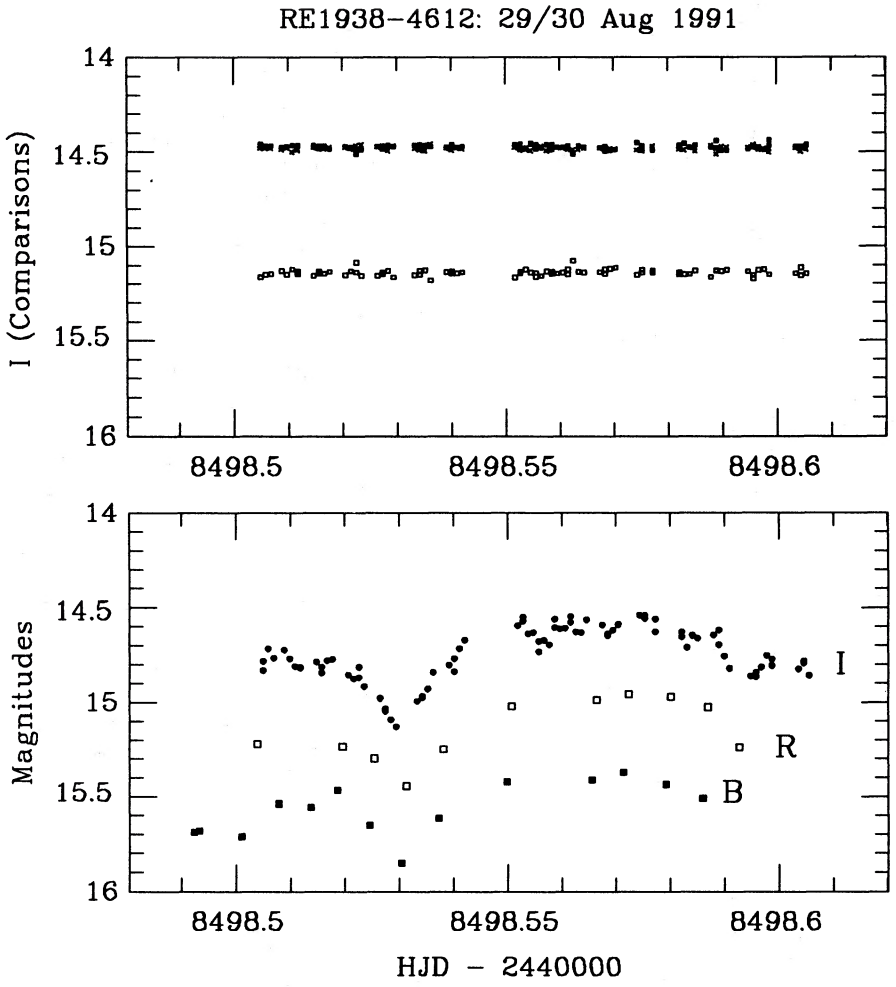

Figure 4. CCD light curves of RE 1938−461 (bottom panel) and three frame standards (top panel) in the B, R_c and I_c filters obtained on 1991 August 29.

vignetting factor, and fraction of instrumental PSF enclosed by the detection cell.

A strong modulation is visible in the EUV light curves, suggestive of a coherent periodicity. We carried out a period search on the EUV data by folding them at all possible independent periods, and testing the folded data against constancy using both the traditional χ^2-statistic, and the L-statistic (Davies 1990). The L-statistic has the distinct advantage of being statistically sound for all sample sizes, the χ^2-squared statistic being an approximation valid only for large sample sizes. The L-statistic also provides a more sensitive way of finding periodicities, as can be seen clearly from the periodograms shown in Fig. 7. This shows that the most significant period as judged by either technique occurs at a period of $18\,350 \pm 120$ s. Although this could be the true EUV period of RE 1938−461, a more likely interpretation is that it represents the beat period between the true period and the period at which the light curve is sampled in the survey 'snap-shots' ($P_{\rm sam} = 5765 \pm 1$ s). In this case the true period is $P_{\rm EUV} = (P_{\rm sam}^{-1} - P_{\rm beat}^{-1})^{-1} = 8406 \pm 25$ s. As we will see, this demonstrates that the EUV period is entirely consistent with the optical photometric and spectroscopic periods, which are identified as the orbital period of the system.

Fig. 8 shows the EUV data for the S1a and S2a filter observations folded at the binary period. The folded light curves for both filters are in phase, and characterized by a high state with phase width ~0.4 and a low state for the remainder of the cycle. The bright part of the cycle is well defined, but does show variability by a factor of ~5 (some of which may be due to flickering, given the unusual way in which the true light curve is sampled in the survey coverage). The EUV count rate in the faint part of the cycle, although much lower, is non-zero and corresponds to around 15 per cent of the average value in the bright phase. We have estimated the epoch of the centre of the EUV bright phase (i.e. approximately EUV maximum) to be HJD 2448160.408 ± 0.005. As will be seen in Sections 6 and 7, the precision of the orbital period determination, based on ~2 months of optical observations in 1991, is insufficient to define the optical phases of the EUV light curve, which was obtained ~1 year earlier.

The filter ratios (i.e. EUV 'colour') in the bright and faint parts of the orbital cycle are the same within measurement uncertainty, the S1a/S2a ratio being 1.24 ± 0.14 in the bright phase. In Fig. 9 we show the region defined by this ratio in the ($N_{\rm H}$, kT) plane, assuming the emission can be characterized by a single-temperature blackbody. Possible values of

kT range from $1-5\times10^5$ K, with N_H in the range $10^{18}-10^{20}$ cm^{-2}.

In light of the fact that many polars exhibit substantial soft X-ray fluxes (e.g. see the review by Lamb 1988), we now estimate likely EUV fluxes of RE 1938−461, based on the spectral parameters. We assume that the EUV flux originates from a blackbody component, also responsible for the soft X-ray flux. The observed average WFC count rates in both the S1a and S2a filters are consistent with a range of blackbody temperatures and column densities, the limits of which are presented in Table 4, together with the unabsorbed bolometric fluxes and luminosities. Also included in the table is the area of the emitting surface, f, in units of the surface area of a standard white dwarf of radius 7×10^8 cm ($M_{wd}\sim0.7\,M_\odot$). The low-temperature limit leads to an unrealistically high luminosity, and radiating area, unless the distance is <100 pc. A more realistic result is achieved for the high-temperature limit, which in fact is what we might have expected for earlier pre-*ROSAT* spectral measurements on polars.

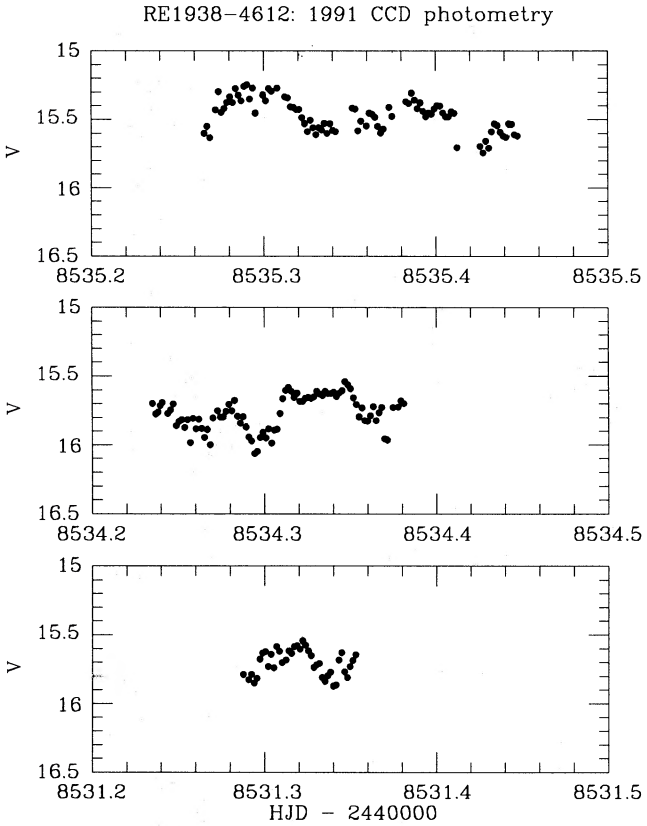

Figure 5. *V*-band CCD light curves of RE 1938−461, obtained on 1991 October 1, 4 and 5.

5 *GINGA* OBSERVATIONS

Hard X-ray observations of RE 1938−461 were made with the *Ginga* LAC (Turner et al. 1989) during the last month of *Ginga* observations before re-entry. The observations took place on 1991 October 5 between 03:00 and 23:00 UT, with 18 700 s exposure time. Observations of a nearby source-free region for background determination were made for about 1 d immediately prior to this. The *Ginga* data were analysed using standard techniques for background subtraction (Hayashida et al. 1989), modified to take account of the lower satellite orbit in late 1991. No significant hard X-ray flux is detected from RE 1938−461 with a 3σ upper limit of 4×10^{-12} erg cm^{-2} s^{-1} in the 2–10 keV band, over which *Ginga* is most sensitive. The upper limit is entirely consistent with the lack of any modulation of the hard X-ray flux at the binary period, for which we can set an upper limit of ~1 count s^{-1}, equivalent to $\sim2\times10^{-12}$ erg cm^{-2} s^{-1} in the 2–10 keV band. We have also checked this result by looking for any variation in the count rate with changing collimator transmission, as is expected if flux is being detected from a point source. No variations were found, giving additional confirmation of the validity of our flux limit.

6 THE PHOTOMETRIC PERIOD

The combined high-speed photometry (including the polarimetry intensity data) and CCD photometry were analysed independently using a discrete Fourier transform (DFT) algorithm, similar to Deeming's (1975). The individual nights

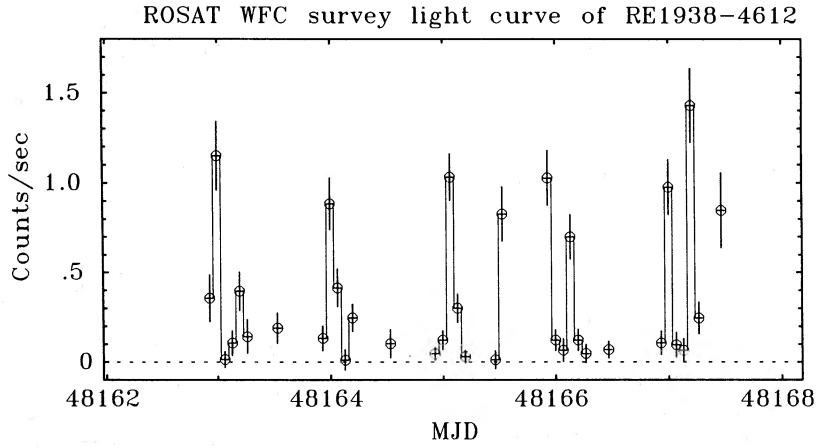

Figure 6. EUV light curve of RE 1938−461 obtained with the *ROSAT* Wide Field Camera between 1990 September 26 and October 3. Points are orbit averages of both the S1a and S2a survey filter data combined.

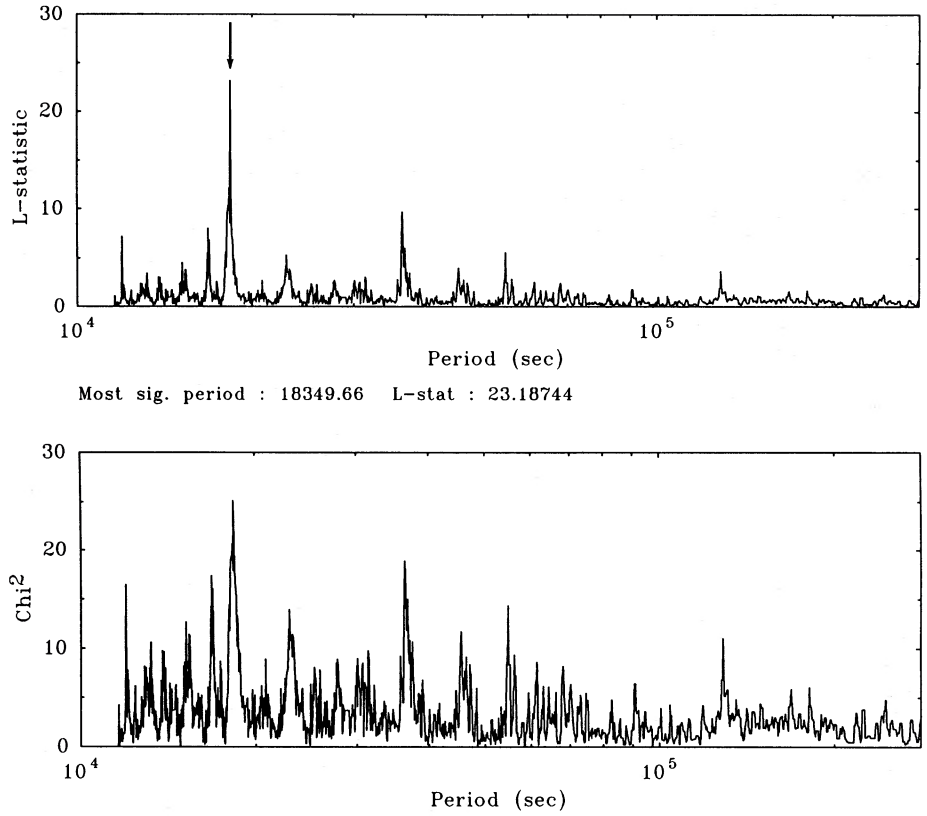

Figure 7. Periodograms of the EUV light curves of RE 1938 − 461, using both the L- (top; Davies 1990) and χ^2-statistics. The most prominent peak occurs at ~ 18 350 s (arrow), and is the beat period between the polar's true orbital period (~ 8401 s) and *ROSAT*'s orbital/spin period (i.e. 5765 s, the sampling period).

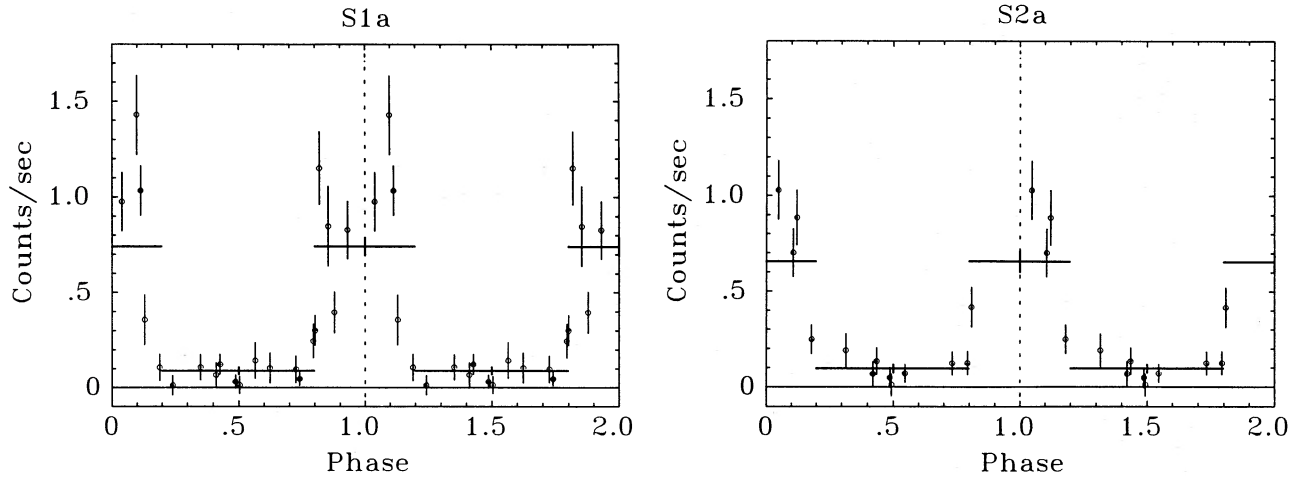

Figure 8. Folded EUV light curves of RE 1938 − 461 through the two survey filters S1a (left-hand panel) and S2a (right-hand panel). Heavy bars are folded data rebinned over broad phase ranges.

were normalized by subtracting, and then dividing by the mean. In Figs 10(a) and (b) we present the Fourier amplitude spectra of these data. The dominant frequencies were at 0.119 02 and 0.119 34 mHz for the high-speed and CCD data sets, respectively. The more accurate high-speed photometry period is completely consistent with the CCD period. Also of note in the DFT spectrum, particularly for the high-speed data (Fig. 10a), are the harmonics of the dominant frequency, up to at least the 4th. A non-linear least squares sinusoidal fit to the high-speed photometry data was made using the fundamental at 0.119 02 mHz and the lowest two harmonics as initial values. The best value for the fundamental frequency from this fit was at $0.119\,025 \pm 0.000\,045$ mHz, or a period of 8401.6 ± 3.2 s (2.3338 ± 0.0009 h). Errors were estimated from the scaled FWHM of the DFT peak, which in the presence of a noisy signal (flickering and

photon noise) is more realistic than a formal fit standard deviation. We adopted a frequency error estimate of $\sim 1/10\,T$, where T is the total time spanned by the data. The two other fitted frequencies agreed to within 0.2 per cent of the harmonics for the fundamental period. Included in Fig. 3 is this fit of three periods, while their amplitudes and phases are given in Table 5. In order to determine the most accurate period possible, a DFT was calculated of the *entire* photometry data set (high-speed and CCD), spanning 58 d (August 8 to October 5). The best period was calculated to be $0.097\,235 \pm 0.000\,016$ d, or 8401.1 ± 1.4 s. An ephemeris was derived from the fit results based on the intensity maxima of the *fundamental* period, and is given as

$$T_{\max}(\mathrm{HJD}) = 244\,8477.4645 \pm 0.0006 + 0.097\,235 \pm 0.000\,016\,E.$$

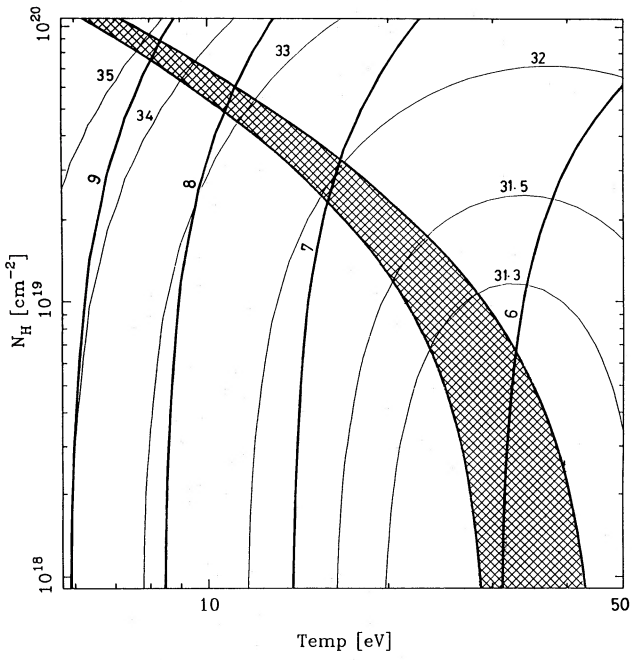

Figure 9. The kT–N_H plane, with the observed filter ratio defining the hatched area, and assuming a single-temperature blackbody. Bold contours show selected values of log R (cm), where R is the radius of an assumed circular emitting region (i.e. $f = \pi R^2/4\pi R_{wd}^2$). Thin contours give the log of the bolometric luminosity. The possible ranges of values are $kT \sim 8$–40 eV and $N_H \sim 10^{18}$–10^{20} cm^{-2}.

7 EMISSION-LINE VELOCITIES: THE SPECTROSCOPIC PERIOD

Radial velocities of the emission lines for both the 1991 August and September observations were determined using both cross-correlation (Tonry & Davis 1979) and double-Gaussian techniques (Schneider & Young 1980; Shafter 1984, 1985). Individual spectra were first 'flattened' to remove the large-scale instrumental and continuum trends. Both Fourier filtering and division by a running mean were used. A template spectrum, consisting of the sum of several individual spectra, was used in the cross-correlation analysis. The derived velocities are therefore an intensity-weighted mean for all the emission lines in the region (i.e. Hγ, He I λ4471 Å and He II λ4686 Å). In Fig. 11 we plot these cross-correlation velocities, together with a least-squares sine fit at the fundamental period, which we will argue is the orbital period of the system.

An identical DFT algorithm was used to derive the amplitude spectrum for these velocities, and it is presented in

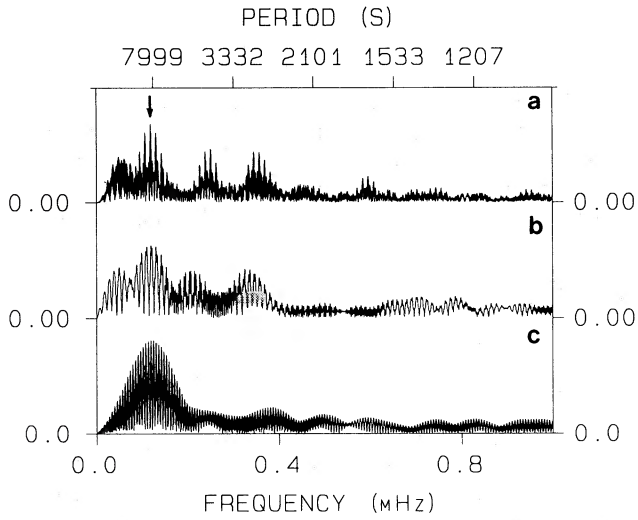

Figure 10. Discrete Fourier transform amplitude spectra for the optical photometry (panels a and b, with intensity ranges 0 to 0.15) and radial velocity variations (panel c, with velocity range 0 to 400 km s^{-1}). The top spectrum applies to the combined high-speed photometry data (including the polarimetry intensities), while the middle panel is for the CCD photometry. A single frequency of 0.119 025 mHz (8401.1 s = 2.33 h), shown by the arrow, is consistent with *all* the data.

Table 4. EUV/soft X-ray blackbody model.

Temperature	kT (eV):	9 (1.04×10^5 K)	39 (4.46×10^5 K)
Absorption Column	N_H (cm^{-2}):	8.2×10^{19}	0.0
Area (w.d. units)	f:	1.36	1.8×10^{-6}
Bolometric flux	F_{bb} (ergs cm^{-2}s^{-1}):	4.67×10^{-8}	2.09×10^{-11}
Bol. luminosity*	$L_{bb} \times d^2$ (ergs s^{-1}):	5.5×10^{34}	2.50×10^{31}

* $\times$ (distance in units of 100 pc)^2.

Table 5. Parameters for photometric and spectroscopic variations.

High-speed Photometry:

Frequency (mHz)	Period (days)	Amplitude	T_{max} (HJD -2440000)
Fundamental:			
0.11903 ±.00005	0.097241 ±.000038	0.1025 ±.0029	8477.3673 ± .0006
Harmonics:			
0.23821 ±.00005	0.048588 ±.000009	0.0648 ±.0029	8477.3755 ± .0005
0.35627 ±.00005	0.032487 ±.000005	0.0591 ±.0030	8477.3559 ± .0003

Cross-correlation velocites

Frequency (mHz)	Period (days)	K (km s^{-1})	T_{max} (HJD -2440000)
0.119087 ±.000042	0.097190 ±.000034	337 ±20	8478.5069 ±.0011

Fig. 10(c). The most significant frequency occurs at 0.119 08 mHz, in close agreement with the photometry result. A single sine fit was made to these velocities, and the K amplitude and phase are included in Table 5. This period is in complete agreement with the optical photometric period, and the ephemeris is given as

$$T_{max}(\mathrm{HJD}) = 244\,8478.5069 \pm 0.0011 + 0.097\,189 \pm 0.000\,034\,E,$$

where T_{max} is the epoch of maximum radial velocity (i.e. redshift).

The large-amplitude ($K \sim 340$ km s^{-1}) radial velocity curve is typical of polars, with occasional large excursions (~ 200–400 km s^{-1}) from the sine fit, which appear to occur at the same phase on the two nights ($\phi_{spec} \sim 0.85$–0.95). However, the most startling aspect of both the velocity and photometric variations is the value of the *period*: namely ~2.33 h. This period is also seen in both the *ROSAT* EUV sky survey light curve and the optical polarimetry, and therefore must be the orbital period of the system. This places RE 1938−461 directly in the CV 'period gap', with a period ~10 per cent longer than UZ For (EXO 033319−2554.2), until now the only polar with an orbital period larger than the 'period spike' polars (Hameury et al. 1987), with periods ~114 min (=1.9 h), while still less than the ~3-h upper limit to the 'gap', which for polars is defined by AM Her itself at 3.09 h.

Results from the double-Gaussian method confirm the above radial velocity variations. This technique, although normally applied to disc systems, is capable of separating the low- and high-velocity regions. For polars this translates to differentiating between gas close to the white dwarf, moving at highest velocities, and gas further out in the accretion stream. In Fig. 12 we show the He II λ4686-Å double-Gaussian radial velocity curve, derived after phase-binning all the spectra using the 2.33-h period. These particular

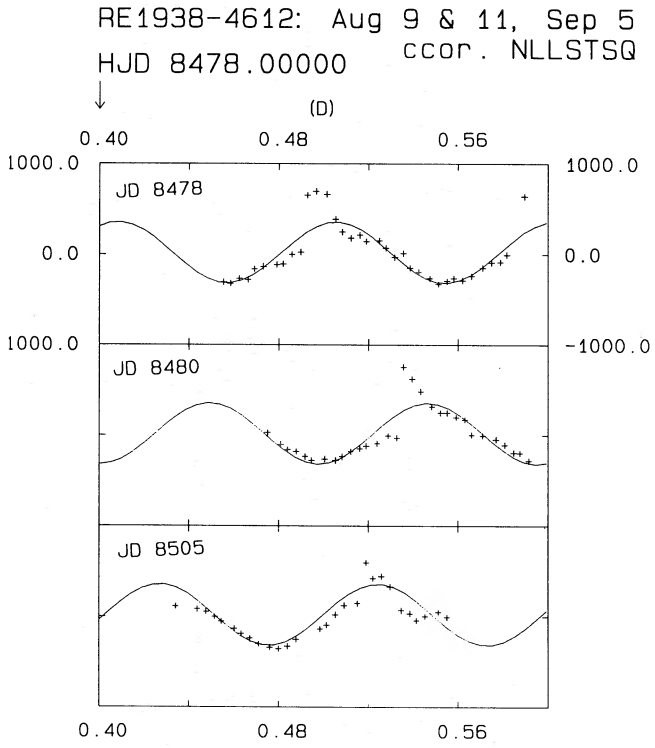

Figure 11. Cross-correlation radial velocity curves of RE 1938−461, together with the best-fitting sinusoid at $P = 0.097\,189$ d. The ordinate ranges from ±1000 km s^{-1}, while the abscissa is in fractional Julian days, as in Fig. 3.

results were for a Gaussian separation of 250–1500 km s^{-1}, and $\sigma = 350$ and 500 km s^{-1}. Results for smaller separations are generally less sinusoidal, and often show large velocity trends. As we will show, this is due to the complex nature of the line profiles, which consist of several components of

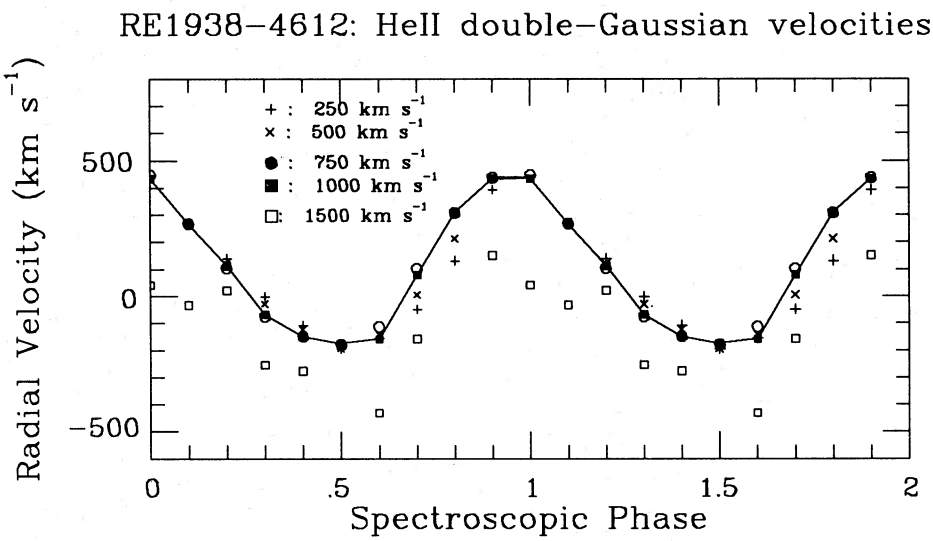

Figure 12. Double-Gaussian convolution He II λ4686-Å radial velocity curve for orbitally binned spectra. The separation of the Gaussians ranged from 250 to 1500 km s^{-1} (see key).

varying velocity amplitudes and phases, which complicate the lower velocity line core. The quasi-sinusoidal variation of the line wings (at ~ 500 km s^{-1} from line centre) is probably due to the overwhelming dominance, at these velocities, of the emission region close to the white dwarf (Liebert & Stockman 1985), where the high-velocity flow is quasi-radial infall. Rotation of the white dwarf, at the orbital period, modulates the projected infall velocities in a sinusoidal manner. A full discussion of the velocity variations is left until Section 10.

8 OPTICAL POLARIZATION AND LIGHT CURVES

After the orbital period was determined from the photometry and spectroscopy, the raw polarimetric data were binned at the orbital period, and the Stokes parameters redetermined. This was done to improve the signal-to-noise ratio, which for the raw data precluded definitive statements on the variations. The results of this are presented in Fig. 13, where both nights' polarization and intensity curves are shown. The spectroscopic ephemeris was used to bin the raw polarization data into 20 bins per orbit for the linear (p) and circular (V) polarizations, and 100 phase bins for the intensities. Both nights show good repeatability, with distinct circular polarization maxima and intensity minima seen each 2.3-h orbital cycle. Although there was some indication in the raw results of variations in the linear polarization, the higher signal-to-noise ratio binned results show little polarization, and no orbital variation in p.

Results from the optical photometry have shown that the light curves of RE 1938−461 appear to show repeatable features from cycle to cycle (see Fig. 3). The intensity varies by ±20–30 per cent of the mean, and two distinct minima in the intensity are observed. We will refer to the slightly deeper, and narrower, minimum as the *primary* minimum. These light curves are somewhat reminiscent of the Type 1, double-humped, EF Eri light curves (Cropper 1985). We

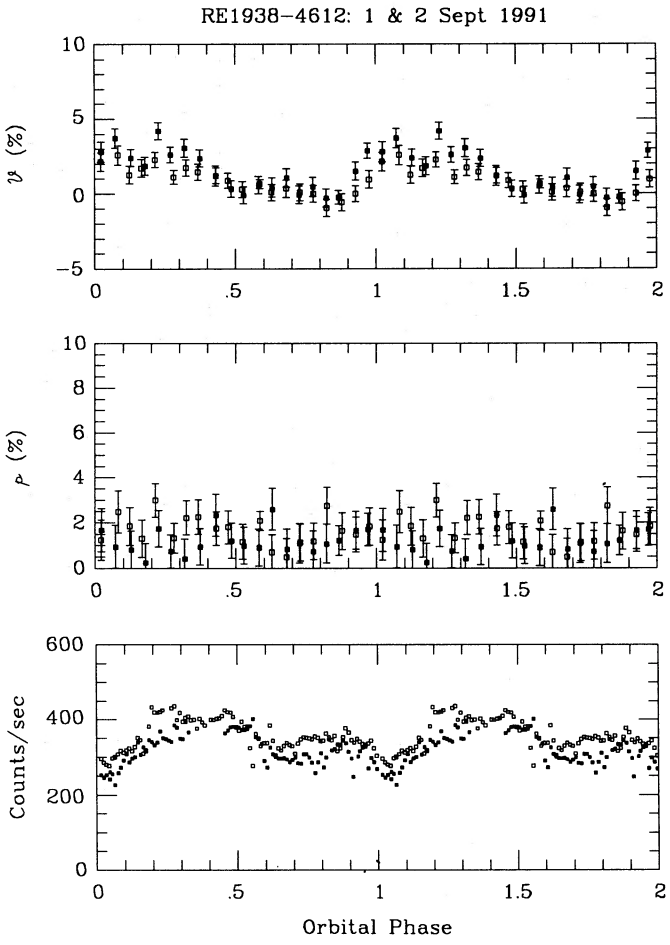

Figure 13. White light polarization and intensity curves for RE 1938−461. The raw data arrays were initially binned (20 bins) on the orbital period before the Stokes parameters were redetermined (see text). Two nights' data on 1991 September 1 (empty squares) and 2 (filled squares) show repeatability in the circular polarizations (V) and intensities.

have subsequently re-binned all of the high-speed photometry at the orbital period, and this averaged light curve is presented in Fig. 14, where we have defined phase zero as the primary minimum observed at HJD 244 8501.449 (see Fig. 3). Clearly the minima are repeatable features, at least during the 1991 season (August to October). The polarization curves from both nights show the same behaviour: a maximum circular polarization (V) occurring just after primary minimum. Interestingly, the primary minima occur at spectroscopic phase ~0.05, i.e. very close to maximum radial velocity. Thus, if the radial velocity curves are dominated by infalling material in an accretion 'funnel', then at primary minimum we are looking down such a funnel, or as collinear as possible. The fact that there is both an intensity minimum and a circular polarization maximum at this time supports this notion. Cyclotron beaming, predominantly perpendicular to the field lines, will result in a flux *minimum* when looking down the fields lines (i.e. accretion column), coincident with a *maximum* in circular polarization. The secondary minimum occurs ~225° in phase *after* primary minimum (at $\phi \sim 0.6$).

9 EMISSION-LINE STRUCTURE

To aid in the interpretation of the orbital (=rotational) variation of the emission-line structures, we have phase-binned both the August and September spectra according to the spectroscopic (radial velocity) ephemeris. Both data sets are similar in showing basically the same profile behaviour. The higher resolution (~1.2 Å) August results, for Hγ and He II λ4686, are seen in Fig. 15, where we have phase-binned according to the spectroscopic ephemeris using 25 bins per orbit, and show two cycles for clarity. Grey-scale images of these phase-binned spectra, at two intensity levels, are also presented in Fig. 16 (opposite). At some phases the FWZI of the lines can extend to ~2000 km s^{-1}, while at times at least two well-separated components are distinctly seen (e.g. at $\phi \sim 0.7$ and 0.8 for Hγ and He II λ4686 Å). Now we can see that this is the cause of the aforementioned (Section 5) velocity 'excursions'. This double or multiple structure is quite typical of polars (e.g. Cowley & Crampton 1977). Mostly the lines exhibit a clear asymmetry, particularly at phases 0.1 to 0.3, where there is an extended high-velocity blueshifted component to the lines. A narrower component (FWHM ~250 km s^{-1}) is also obvious at times, particularly for He II λ4686 (e.g. $\phi = 0.1$), and this can be traced through virtually all phases.

Qualitatively, the emission-line morphology and variability resemble that observed in many other polars (e.g. Schneider & Young 1980; Crosa et al. 1981; Liebert & Stockman 1985; Mukai & Charles 1985; Mukai et al. 1986; Rosen, Mason & Córdova 1987). In particular, there are specific similarities between our grey-scale plots of RE 1938−461 and those of V834 Cen (E 1405−451), derived by Rosen et al. (1987). In the latter, four distinct velocity components could be identified, at least over part of the orbital cycle. These were referred to by Rosen et al. (1987) as the broad-base, medium-velocity (MVC), high-velocity (HVC), and narrow components. In contrast, we can only clearly identify three components in RE 1938−461, which we refer to as the broad, core, and high-velocity components. As we will show, these are very similar to the first three components identified in V834 Cen.

As in other polars, the broad, or base, component extends well out in velocity into the line wings. Our double-Gaussian convolution results, for the widest separations (Section 7; Fig. 12), essentially map out the velocity variations of these wings. However, because of possible contamination (e.g. from the high-velocity component at certain phases) of these results, we have independently derived the centroid

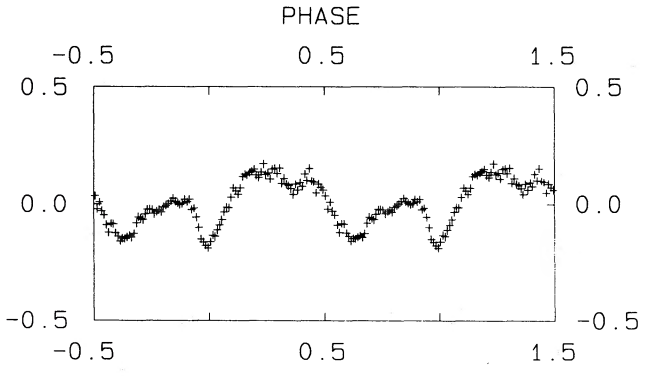

Figure 14. The average phase-binned (100 bins) white light curve for RE 1938−461, from all data obtained in 1991 (August to September). Note the presence of two minima per cycle (see text).

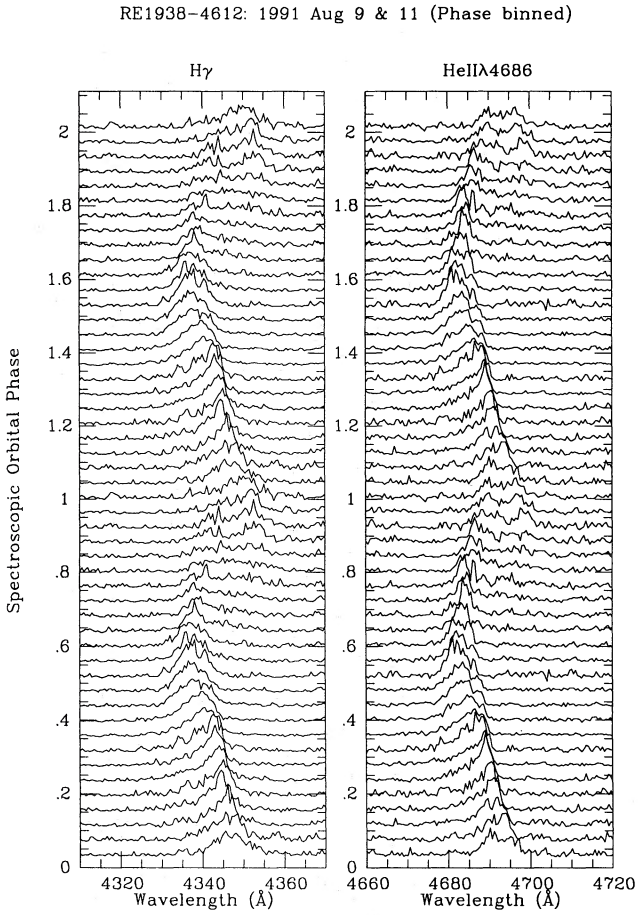

Figure 15. Orbital variations in the Hγ and He II λ4686-Å emission-line profiles. Two cycles are shown for clarity.

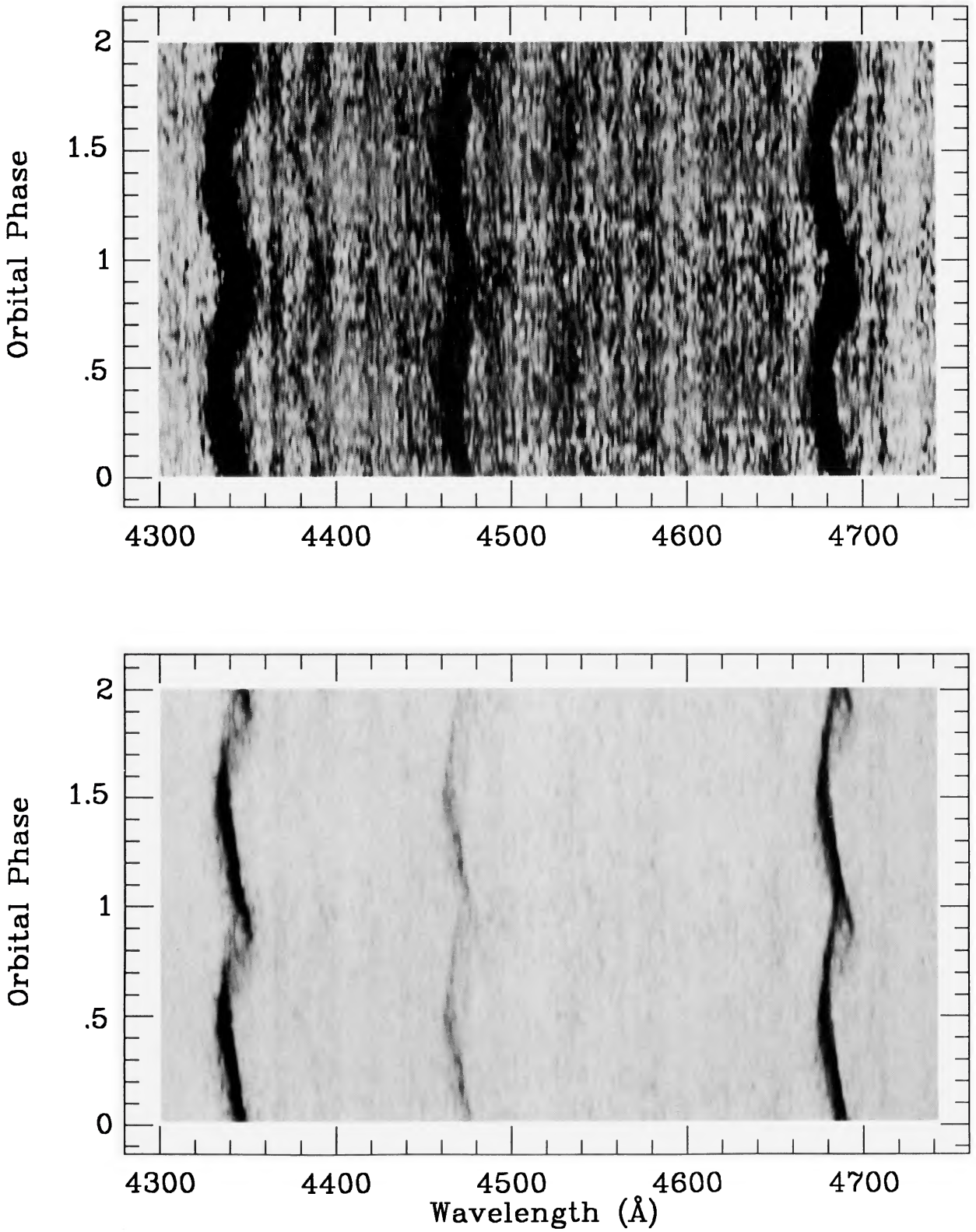

Figure 16. Two grey-scale images of the phase-binned spectra of RE 1938−461 showing, from left, the Hγ, He I λ4471-Å and He II 4686-Å lines, and at two different intensity levels. The top and bottom panels show best the broad and core components, respectively. The high-velocity component can be seen between phases 0.75 and 1.00 as an extension to the red edge, resulting in line doubling at these phases. A useful comparison can be made with the grey-scale plots of V834 Cen by Rosen et al. (1987).

velocities of the broad component, and at the same time estimates of the line FWZIs, for both the Hγ and He II λ4686 lines. An eye estimate was made of both the blue and red limits of the line profile, where they just merged into the continuum. The resulting velocity and FWZI curves of the broad component are presented in Fig. 17. Both the amplitudes and phases are quite similar to the double-Gaussian results. Importantly, the results also confirm that *both* radial velocity curves exhibit large positive gamma velocities of ~ 200–400 km s^{-1}. The implication of this result, in terms of the likely accretion geometry of RE 1938 − 461, is discussed in Section 10.3.

What is also quite obvious from our grey-scale plots (Fig. 16; opposite p. 104) is that the radial velocity variations of the bright core component are distinctly out of phase with the broad component, lagging by about 0.2 in phase. This is confirmed by independent measurements of the core centroid, from either measuring a line's brightest pixel in the grey-scale image, or estimating the position of the peak of the line profile by eye. Both methods produce radial velocity curves (Fig. 17) lagging in phase by ~0.2. The result is reminiscent of V834 Cen (Rosen et al. 1987), where the medium-velocity component (MVC) was similarly out of phase (by ~0.2) with the broad base. The final similarity between RE 1938 − 461 and V834 Cen concerns the so-called high-velocity component (HVC), which, as in V834 Cen, is only observed at certain orbital phases, and appears as an extension of the broad-base component. In RE 1938 − 461, this component is most obvious near $\phi \sim 0.75$–1.00, where a distinctly redshifted component (~900 km s^{-1}) causes the lines to double. This contrasts with the result of Rosen et al. (1987) for V834 Cen, in which their HVC appears as a *blueshifted* component.

Finally, despite probably adequate spectral resolution, there is no indication in RE 1938 − 461 of a narrow component attributable to the X-ray heated face of the secondary star.

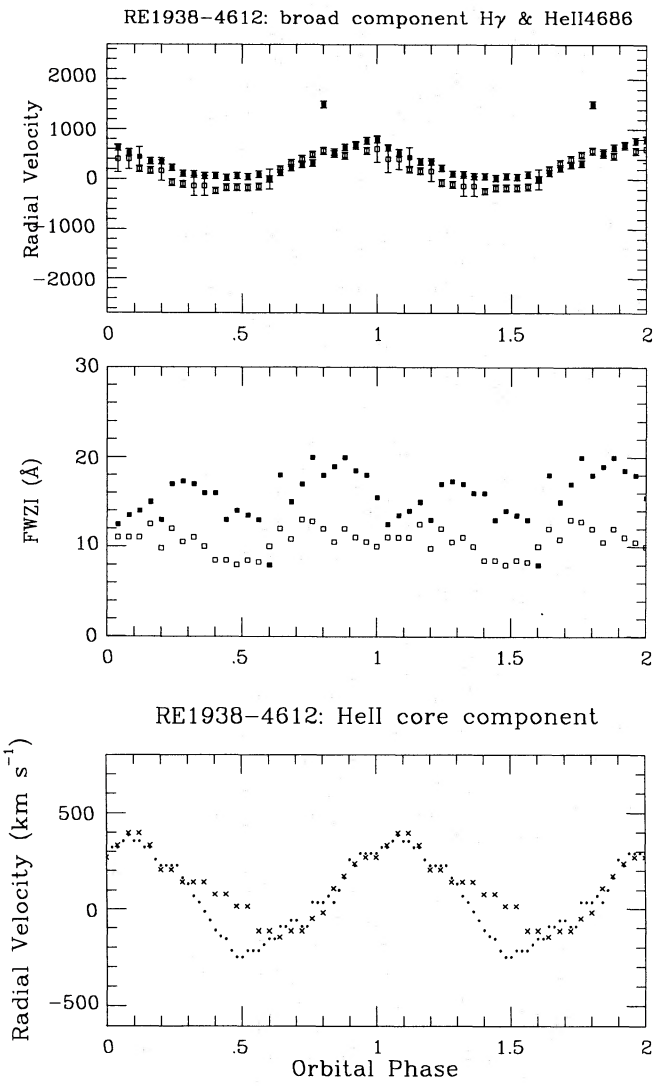

Figure 17. Comparison between the radial velocity curves derived for the broad (top panel) and core (bottom panel) components of the emission lines. Results for both Hγ (empty boxes) and He II λ4686 Å (filled boxes) are shown for the broad component, while only the He II core result is shown, but using two different techniques to estimate the position: brightest pixel (dots) and peak-of-profile (crosses). The middle panel shows how the FWZI varies for the broad component of the lines (Hγ: empty boxes; He II: filled boxes).

10 DISCUSSION

10.1 The orbital period and evolutionary considerations

We have unequivocally determined that the orbital period of RE 1938 − 461 is 0.097 235 ± 0.000 016 d (2.33 h). This period is entirely consistent with the *ROSAT* EUV observations, the optical photometry, polarimetry and spectroscopy.

Currently, the widely accepted explanation for the CV period distribution, and particularly the dearth of systems in the 2–3-h period 'gap', involves the secular evolution of CVs towards shorter orbital periods as a result of the loss of orbital angular momentum. For systems with periods > ~3 h, the dominant loss mechanism is thought to be magnetic braking by the secondary's magnetic field and wind (e.g. Verbunt & Zwaan 1981; Mestel & Spruit 1987). At periods near 3 h, this mechanism becomes so inefficient that the time-scale for mass transfer becomes larger than the secondary's thermal time-scale, allowing the star to relax to thermal equilibrium, detaching from its Roche lobe and ceasing mass transfer altogether (e.g. Ritter 1985). The 3-h upper limit to the gap is probably a result of the Roche lobe filling secondaries becoming fully convective (Spruit & Ritter 1983; Rappaport, Verbunt & Joss 1983), whereupon their magnetic activity, or more likely their stellar winds, decrease markedly (Hameury et al. 1987). Thereafter the dominant angular momentum loss mechanism is through gravitational radiation (e.g. Faulkner 1971; Paczyński & Sienkiewicz 1981; Rappaport, Joss & Webbink 1982), but it is not until the orbits have shrunk to periods of ~2 h that the secondaries re-attach to their Roche lobes, and mass transfer resumes. This above scenario, described as disrupted magnetic braking (e.g. Lamb & Melia 1986), is able to reproduce quantitatively both the period distribution (including the gap) and the mass transfer rates observed (Lamb & Melia 1988).

Of the 17 polars known prior to the discovery of RE 1938 − 461, 13 (76 per cent) of them have periods below the ~3-h upper limit of the CV period gap. This period

distribution is significantly different from CVs as a whole (e.g. Schmidt & Liebert 1987), and even from the non-synchronized magnetic intermediate polars, which generally have orbital periods above the gap. Furthermore, there is a very significant clustering of polar periods at ~114 min (Morris et al. 1987). This significant 'spike' in the period distribution, which is very narrow ($\langle P\rangle = 114.18$ min, $\sigma = 0.54$ min), contains ~40 per cent of *all* polars below the gap. The period spike is a likely consequence of the enhanced chances of detection of systems at the lower edge of the gap, in which the convective secondaries have just re-attached to their Roche lobes after crossing the period gap. At this stage the mass transfer rates, and hence the accretion luminosities, are higher than at subsequent epochs because the mass-loss time-scale for the envelope is shorter than the secondary's thermal time-scale (e.g. Lamb & Melia 1988). This fact, coupled with the initially slower period-evolution (initially increasing to slightly longer periods as the secondary is driven far out of thermal equilibrium; thereafter a secular decrease in the period), results in systems 'congregating' at the spike period of ~114 min. The existence of such an obvious spike has led to strict limits being put on both the white dwarf masses and parameters describing the secondaries: specifically their entropy, opacity and density structures (e.g. Hameury et al. 1988; Hameury, King & Lasota 1990, 1991). Hameury, King & Lasota (1988) show that the white dwarf masses of the spike members, and indeed *most* polars, are 0.6–0.7 $M_\odot$. Similarly, Ritter & Kolb (1992) not only conclude that the white dwarf masses are in a narrow range, and >0.7 $M_\odot$, but that the secondaries *also* have a narrow mass dispersion, and are born with masses >0.5 $M_\odot$. The origin for the restricted white dwarf mass range in polars is unclear, although it is probably connected to their magnetic nature, and the apparent restricted range in magnetic field strengths, which may somehow act to suppress mass loss in nova explosions (Hameury et al. 1989). An absence of a similar period spike in the majority of (non-magnetic) CVs is then just a consequence of the extended range of white dwarf primary masses, which act to smear out such a spike in the period distribution. Since the white dwarf masses mostly define the upper and lower limits to the period gap, and hence the exact position of a period spike, a *variation* in these masses will lead to variations in these period limits. Each individual system will have its own 'personal' gap and spike period, defined by its white dwarf mass. A continuum of white dwarf masses leads to less sharp gap boundaries and, most importantly, a 'smeared out' period spike, representative of the distribution as a whole.

Whereas in the above scheme a large fraction of polars (~50 per cent or more) is required to have these restricted white dwarf masses for the period spike to be present at all, it is still statistically possible for *individual* systems to have higher (or lower) masses. Such systems will have different limits to their 'personal' gaps, and for higher masses will come back into contact below the gap at periods above the 114-min spike period. For systems born with periods only just above ~4 h, nova explosions might not remove the same amount of mass as in the majority of (initially longer period) polars, and they may therefore have somewhat larger white dwarf masses, and hence end up with periods somewhat above the 114-min spike value, when they resume mass transfer again below the gap. A potential objection to the above scenario is that, while the spike is absent in 'normal' CVs, the period gap is still very evident, and with apparently fairly distinct boundaries.

There is some indication that the hitherto longest period (i.e. before the discovery of RE 1938−461) polar below the period gap, UZ For (EXO 033319−2554.2), with a period of 2.1 h (126 min), has a significantly larger white dwarf mass than the spike members, with an initial estimate by Beuermann, Thomas & Schwope (1988) of ~0.9 $M_\odot$. Recently, however, Bailey & Cropper (1991) have deduced an upper limit of 0.8 $M_\odot$, based on their detailed eclipse observations. Whereas Hameury, King & Lasota (1988) conclude that UZ For's white dwarf mass has to be 1.2–1.3 $M_\odot$ for their evolutionary theory to be self-consistent, their more conservative conclusion is that it is really only sufficient that the UZ For white dwarf be *more* massive by between 0.25 and 0.65 $M_\odot$ in comparison to the spike members.

In the case of RE 1938−461, its orbital period of 140 min (2.33 h) is difficult to reconcile with evolution through the period gap from an initial period of >4 h or so. Hameury, King & Lasota (1988) concluded that, accounting for uncertainties in the secondary models, and specifically the entropy and opacity structure, an upper limit for the periods of systems below the period gap was ~131 min, and this was for systems with an upper limit Chandrasekhar white dwarf mass (1.44 $M_\odot$). Only for unlikely values of the wind density index, n, in the Mestel & Spruit (1987) braking law, *and* for a high white dwarf mass (e.g. Hameury et al. 1991), is it possible for RE 1938−461 to evolve through the gap, as other polars do. A far more likely explanation, which does not require particularly contrived conditions, is that RE 1938−461 was *born* in the period gap. There is nothing particularly unusual or surprising in this, and in fact it is probably more significant that such born-in-gap systems have not been found until now. The evolutionary tracks in the *period–$\dot{M}$* diagrams of such objects are quite different from systems which first become semi-detached binaries above the period gap (e.g. Hameury et al. 1991). Such CVs may initially evolve to *longer* periods before the secondaries become fully convective, detach from their Roche lobes, and cease mass transfer until below the period gap. The initial conditions (e.g. component masses) will determine these tracks, as well as the periods at which mass transfer ceases/resumes, i.e. will define the 'gap' and 'spike'. Any system born with a period between 2.7 and 3.5 h will reappear, after crossing its own period gap, at ~2.5 h, before secularly evolving to a shorter period again (Hameury et al. 1991). It is quite feasible that RE 1938−461 is such a system, and in this sense it has had, and will continue to have, a somewhat different evolutionary history from most of the other polars, which evolve from longer periods (>4 h), cross the period gap and re-attach at or very close to the spike period, therefore evolving to shorter periods.

It is interesting that another polar recently discovered from the *ROSAT* survey has an orbital period of 125 min. With this system, UZ For and now RE 1938−461, it appears that the period distribution is filling out to that of the non-magnetic distribution, although the spike remains a significant feature not seen in the latter. To draw significant conclusions based on the differences between the two distributions is a risky business, however, in light of the strong selection effects which often come into play. Such a

flux-limited sample as the *ROSAT* survey may help in addressing possible biases, notwithstanding the high non-uniformity of the local interstellar absorption.

10.2 The soft X-ray/EUV excess

To evaluate the degree of any soft X-ray/EUV excess, we adopt the more realistic high-temperature limit of the EUV spectral fit (Table 4), which leads to a conservative (i.e. the lowest) blackbody bolometric flux of $\sim 2.1\times10^{-11}$ erg cm^{-2} s^{-1}. For the hard bremsstrahlung component, we take the *Ginga* upper limit for the 2–10 keV flux of $\sim 4\times10^{-12}$ erg cm^{-2} s^{-1}. For a reasonable temperature of between 10 and 20 keV for the bremsstrahlung component, the bolometric correction for the hard component is ~ 2. This implies a *minimum* soft-to-hard X-ray flux ratio of $2.1\times10^{-11}/2\times4\times10^{-12}\sim2.5$. This lower limit establishes that RE 1938−461 exhibits a clear soft X-ray excess, and the true ratio is very likely to be much higher, since a more realistic blackbody temperature of ~ 30 eV and a reasonable column density of a few times 10^{19} cm^{-2} might be expected. In addition, the *Ginga* result is only an upper limit to the hard X-ray flux.

An estimate of the optical flux can be derived from the observed mean V magnitude of ~ 15.6, which implies a 5000–6000 Å flux ($f_{\rm opt}$) of $\sim 2\times10^{-12}$ erg cm^{-2} s^{-1}. The X-ray-to-optical flux ratios are therefore <2 for the hard component [$f_{\rm hard\,X}(2\text{–}10\ {\rm keV})/f_{\rm opt}$], and >10 for the EUV component ($f_{\rm EUV}/f_{\rm opt}$). If we adopt the same arguments as used by Patterson (1981), we derive a pseudo-bolometric optical flux of $\sim 4\text{–}8\times10^{-11}$ erg cm^{-2} s^{-1} (depending on the bolometric correction), applicable to the region contributing most of the *optical* luminosity. This implies that the ratio of *bolometric* luminosities (EUV to optical) is $>0.3\text{–}0.5$, although the assumption of a single-temperature region responsible for *all* of the optical luminosity may negate this.

10.3 Accretion geometry

The radial velocity variations, and the structure of the emission lines (discussed in Sections 7 and 9), indicate that the velocities arise from accreting material flowing pseudo-radially on to, or near, the magnetic poles of the white dwarf. Both the velocity amplitudes and phase offsets between the core and broad components are suggestive of stream curvature, with the higher velocity material presumably arising closer to the white dwarf. From the large γ-velocities observed, it would appear that the accreting pole responsible for the line emission is mostly confined to the observer's hemisphere, namely $i+\beta<90°$ over most of the orbital cycle (where, as usual, i is the orbital inclination and β the magnetic colatitude of the accretion region). This conclusion is also supported by the circular polarization (V) curve, which is positive for ~ 60 per cent of the orbit, and approaches zero, even possibly reversing sign (although this is only a $2\text{–}3\sigma$ result) for a short period at minimum ($\phi_{\rm spec}\sim0.8\text{–}0.9$), indicating that part of the accretion funnel rotates over the limb of the white dwarf. It may be significant that, at this same phase, the so-called high-velocity line component is most evident. We finally comment on the variation in the line FWZIs as a function of orbital phase. Although the method used to measure these was rather crude, it appears that for both Hγ and He II λ4686 the FWZI peaks twice during an orbital cycle, with maxima at $\phi\sim0.25$ and 0.75 (Fig. 17). Such behaviour is fully consistent with the notion of an accretion funnel, which might be expected to have two maxima in the line width when the funnel is viewed side-on twice during the orbit, when the differences between the velocity extremes are greatest (e.g. Ferrario, Wickramasinghe & Tuohy 1989, and references therein).

In contrast to the line emission and polarization curves, the EUV light curve (Section 4; Fig. 8) has only a ~ 40 per cent duty cycle, with the EUV flux only just detectable for the majority (i.e. 60 per cent) of the orbital cycle. This indicates that the accretion region responsible for the bulk of the EUV/soft X-ray emission is mostly hidden from view behind the limb of the white dwarf, i.e. $i+\beta>90°$ for most of the cycle. Unfortunately, as has already been said, it is not yet possible to phase the EUV light curve on the optical ephemeris, due to uncertainties in the value of the orbital period. Therefore we cannot as yet determine the phase (i.e. angular) offset between the two accretion regions.

It therefore appears that RE 1938−461 is a two-pole system, with the secondary pole responsible for the bulk of the EUV/X-ray emission. Such two-pole scenarios are often seen in polars, for example when AM Her itself is in its enhanced 'soft' phase (e.g. Beuermann 1988). The primary pole in RE 1938−461 would therefore emit most of the cyclotron (polarized) emission, and be responsible for most of the line emission further out in the stream. The structure of the optical light curve (double-humped) is consistent with such a two-pole interpretation, while the low degree of polarization (circular and linear) might be a result of dilution effects. That both poles contribute to the optical emission is demonstrated by the fact that the light curve does not exhibit a 'faint phase', as in ST LMi (Cropper 1986).

10.4 Summary

RE 1938−461 has been identified as a new $V\sim15.6$ AM Herculis binary (polar), with an orbital period of 2.33 h. It exhibits all the usual hallmarks of polars: a large degree of line excitation and high velocities, a substantial soft X-ray flux and (albeit low) variable circular polarization. In addition, RE 1938−461 was the EUV-brightest of *any* polar seen during the *ROSAT* sky survey by the WFC. Its orbital period (in the gap) could be the result of the evolution of a system containing a particularly massive white dwarf primary, which has just re-established contact after evolving through the period gap. However, this scenario requires rather unusual parameters, and a far more likely explanation of the evolutionary status of RE 1938−461 is that it was born *in situ*, i.e. first became a semidetached binary in the gap. The optical and EUV light-curve structure, the nature of the polarization and the velocity curves all indicate that RE 1938−461 has two accreting poles, the secondary pole responsible for most of the EUV/X-ray emission, and the primary dominant in the optical region. Finally, like many polars, RE 1938−461 exhibits a substantial soft X-ray excess, exceeding the hard bremsstrahlung component by at least a factor of 2, and probably a lot more.

ACKNOWLEDGMENTS

We are extremely grateful for fruitful discussions with both Andrew King and Jean-Pierre Lasota. Paul Barrett helped to provide some of the polarization acquisition/reduction code and gave valuable advice, for which we thank him. Paul Schechter kindly provided the DoPHOT CCD reduction package, which is supported through NSF grant AST 83-18504. KOM acknowledges the support of the Royal Society. Again we are grateful for the excellent support of the SAAO staff, and particularly Isobel Bassett, for help with CCD reductions.

REFERENCES

Bailey J., Cropper M., 1991, MNRAS, 253, 27
Beuermann K., 1988, in Coyne G. V., Moffat A. F., Tapia S., Mogalhaes A. M., Schulte-Ladbeck R. E., Wickramasinghe D. T., eds, Polarization of Circumstellar Origin. Vatican Observatory, Vatican City, p. 125
Beuermann K., Thomas H. C., Schwope A., 1988, A&A, 195, L15
Cowley A. P., Crampton D., 1977, ApJ, 212, L121
Cropper M., 1985, MNRAS, 212, 709
Cropper M., 1986, MNRAS, 222, 853
Cropper M., 1990, Space Sci. Rev., 54, 195
Crosa L., Szkody P., Stokes G., Swank J., Wallerstein G., 1981, ApJ, 247, 984
Davies S. R., 1990, MNRAS, 244, 93
Deeming T. J., 1975, Ap&SS, 36, 137
Faulkner J., 1971, ApJ, 170, L99
Ferrario L., Wickramasinghe D. T., Tuohy I.R., 1989, ApJ, 341, 327
Hameury J. M., King A. R., Lasota J. P., Ritter H., 1987, ApJ, 316, 275
Hameury J. M., King A. R., Lasota J. P., 1988, A&A, 195, L12
Hameury J. M., King A. R., Lasota J. P., Ritter H., 1988, MNRAS, 231, 535
Hameury J. M., King A. R., Lasota J. P., Livio M., 1989, MNRAS, 237, 835
Hameury J. M., King A. R., Lasota J. P., 1990, MNRAS, 242, 141
Hameury J. M., King A. R., Lasota J. P., 1991, A&A, 248, 525
Hayashida K. et al., 1989, PASJ, 41, 345
King A. R., Hameury J. M., Lasota J. P., 1990, in Mauche C. E., ed., Accretion-Powered Compact Binaries. Cambridge Univ. Press, Cambridge, p. 439
Lamb D. Q., 1988, in Coyne G. V., Moffat A. F., Tapia S., Mogalhaes A. M., Schulte-Ladbeck R. E., Wickramasinghe D. T., Polarization of Circumstellar Origin. Vatican Observatory, Vatican City, p. 151
Lamb D. Q., Melia F., 1986, in Mason K. O., Watson M. G., White N. E., eds, Physics of Accretion onto Compact Objects. Lecture Notes in Physics, Vol. 226, Springer-Verlag, Berlin, p. 113
Lamb D. Q., Melia F., 1988, in Coyne G. V., Moffat A. F., Tapia S., Mogalhaes A. M., Shulte-Ladbeck R. E., Wickramasinghe D. T., Polarization of Circumstellar Origin. Vatican Observatory, Vatican City, p. 45
Liebert J., Stockman H. S, 1985, in Lamb D. Q., Patterson J., eds, Cataclysmic Variables and Low Mass X-ray Binaries. Reidel, Dordrecht, p. 151
Mason K. O. et al., 1991, Vistas Astron., 34, 343
Mateo M., Schechter P. L., 1989, in Grosbøl P. J., Murtagh F., Warmels R. H., eds, ESO Conf. Workshop Proc. No. 31, 1st ESO/ST-ECF Data Analysis Workshop. ESO, Garching, p. 69
Menzies J. W., Cousins A. W. J., Banfield R. M., Laing J. D., 1989, S. Afr. Astron. Obs., Circ., 13, 1
Mestel L., Spruit H. C., 1987, MNRAS, 226, 57
Morris S. L., Schmidt G. D., Liebert J., Stocke J., Gioia I., Maccacaro T., 1987, ApJ, 314, 641
Mukai K., Charles P. A., 1985, MNRAS, 212, 609
Mukai K., et al., 1986, MNRAS, 221, 839
Paczyński B., Sienkiewicz R., 1981, ApJ, 248, L27
Patterson J., 1981, Nat, 292, 810
Pounds K. A. et al., 1993, MNRAS, 260, 77
Rappaport S., Joss P. C., Webbink R. F., 1982, ApJ, 254, 616
Rappaport S., Verbunt F., Joss P. C., 1983, ApJ, 275, 713
Ritter H., 1985, A&A, 145, 227
Ritter H., Kolb U., 1992, A&A, 259, 159
Rosen S. R., Mason K. O., Córdova F. A., 1987, MNRAS, 224, 987
Schmidt G. D., 1988, in Coyne G. V., Moffat A. F., Tapia S., Mogalhaes A. M., Schulte-Ladbeck R. E., Wickramasinghe D. T., Polarization of Circumstellar Origin. Vatican Observatory, Vatican City, p. 85
Schmidt G. D., Liebert J., 1987, A&AS, 131, 549
Schneider D. P., Young P., 1980, ApJ, 238, 946
Shafter A. W., 1984, AJ, 89, 1555
Shafter A. W., 1985, in Lamb D. Q., Patterson, J., eds, Cataclysmic Variables and Low Mass X-ray Binaries. Reidel, Dordrecht, p. 355
Spruit H. C., Ritter H., 1983, A&A, 124, 267
Tonry J., Davis M., 1979, AJ, 84, 1511
Tuohy I. R., Ferrario L., Wickramasinghe D. T., Hawkins M., 1988, ApJ, 328, L59
Turner M. J. L. et al., 1989, PASJ, 41, 345
Verbunt F., Zwaan C., 1981, A&A, 100, L7
Wells A. et al., 1990, Proc. SPIE, 1344, 230
Wickramasinghe D. T., 1988, in Coyne G. V., Moffat A. F., Tapia S., Mogalhaes A. M., Schulte-Ladbeck R. E., Wickramasinghe D. T., eds, Polarization of Circumstellar Origin. Vatican Observatory, Vatican City, p. 3